IEEE Open Journal of
Antennas and Propagation

Received 23 August 2021; revised 24 September 2021; accepted 18 October 2021. Date of publication 21 October 2021;
date of current version 15 November 2021.

Digital Object Identifier 10.1109/OJAP.2021.3121805

Analytic Sinusoidal Steady-State Electromagnetic Field Expressions for the Ideal Veselago Lens

MARZIEH EINI KELESHTERI (Graduate Student Member, IEEE),
VLADIMIR I. OKHMATOVSKI (Senior Member, IEEE), AND JOE LOVETRI (Senior Member, IEEE)

Department of Electrical and Computer Engineering, University of Manitoba, Winnipeg, MB R3T 5V6, Canada

CORRESPONDING AUTHOR: M. EINI KELESHTERI (e-mail: einikelm@myumanitoba.ca)

This work was supported by the Natural Sciences and Engineering Research Council of Canada (NSERC).

ABSTRACT Analytic expressions for the sinusoidal steady-state electromagnetic field associated with an ideal Veselago lens illuminated by either a line-source (2D case) or an electric dipole point-source (3D case) are obtained based on power flow considerations and the imposition of appropriate boundary conditions. The fields are written in terms of the standard free-space Green's function except that both incoming and outgoing waves are utilized. Expressions for the Poynting vector are also provided. Some components of the field suffer a complex-conjugate discontinuity across two *power-transfer singularity planes*, one within the lens and one through the external focus point, so named because all the power generated by the point-source transfers through a singular point on each plane. The internal *power-transfer singular point* and the illuminating point-source are equidistant from the first lens boundary, whereas the external singular point, i.e., the focus point, and the internal singular point are equidistant from the second lens boundary. These singularities represent different physical properties than the traditional source or sink singularities. The new interpretation based on the concise analytic field expressions clears up the physically objectionable interpretation of these singularities as representing new sources of energy: no new sources of energy exist in our representations.

INDEX TERMS Double-negative, green's function, metamaterials, Veselago lens.

I. INTRODUCTION

THE POSSIBILITY of materials with simultaneously negative permittivity (ϵ) and permeability (μ) and different physical properties from materials with positive ϵ and μ was cast in 1968 by Victor G. Veselago [1]. Although he stated that no such materials were known to exist naturally at the time of his research, he provided the unique physical properties such materials would have. He called these left-handed materials (LHM) based on the fact that the wave vector $\bar{k}$, the electric field vector $\bar{E}$, and magnetic field vector $\bar{H}$ for a plane-wave in such materials construct a left-handed system. Veselago did mention that at some particular frequencies some dispersive substances such as plasmas could take on negative values for both parameters. Most interestingly, Veselago noticed that a planar slab of LHM is capable of focusing waves.

Now commonly referred to as the Veselago Lens (VL), consider a slab of width d as is shown in Fig. (1). He justified the focusing phenomenon mathematically by introducing a negative index of refraction n. Using a ray-based model he showed that the diverging rays from a point-source A located at distance $l < d$ from the first interface of the VL are reversely refracted on the first boundary of the lens and converge onto a focus point B inside the VL the same distance l from the first interface. Subsequently, the diverging rays from the internal focus point B are reversely refracted at the second boundary of the VL and converge at the second focus point C located on the other side of the lens a distance $2d$ away from the point-source A, [1]. Using a plane wave model and a spectral-domain decomposition of a point-source Pendry [2] emphasized that a lens made of a metamaterial having $\epsilon_r = \mu_r = -1$ will perfectly focus waves emanating from a point-source. He proved that the evanescent waves are amplified while being transmitted inside the lens so that even fine details of an object will be restored creating a perfect image of the object on the other side. He also showed that the reflection coefficient becomes

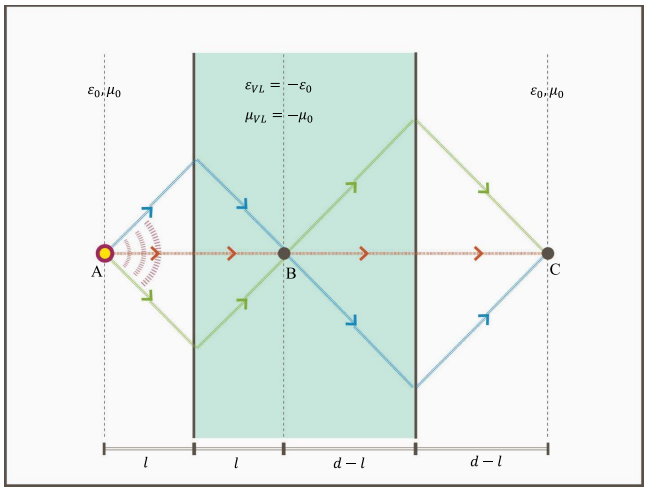

FIGURE 1. Focusing waves by negative refraction (as in [1]).

zero and that the transmission coefficient is equal to one for all plane-wave components.

Pendry also prescribed a practical approach for creating an almost super lens using a slab made of silver with a complex permittivity and negative real part. Although double-negative substances have not been found in nature, over the past two decades Pendry's paper has spurred on significant research attempting to artificially engineer metamaterials exhibiting such properties. Apparently, Smith, *et al.* were the first team to successfully engineer metamaterials with a negative index of refraction in 2000 and 2001, [3], [4]. The work was summarized in [5], where the idea for creating materials with a negative index of refraction was reaffirmed. Several other experimental attempts have been made and a summary can be found in [6], [7].

Pendry's results evoked many critiques from different groups of scientists, some implying that no such lens could exist, [8], [9], and others claiming that a perfect lens could be made of metamaterials only approximating the ideal lens using lossy or frequency dispersive metamaterials which would reduce imaging resolution, [5], [10]–[13]. Many of these critiques are based on the analytic form and interpretation of the expressions describing the electromagnetics of the ideal VL. Unfortunately, most previous mathematical expressions of the ideal VL have been in terms of spectral-domain representations. Therefore, interpretations on the physical realizability of such a lens can be quite complicated[1]. In this paper we provide explicit mathematical characterizations in terms of well-established analytic functions for the fields of the ideal VL illuminated by sinusoidal steady-state point-source. We believe that the interpretation of the physics and speculation on the physical realizability of such a super lens is better performed using these representations. In addition, the numerical evaluation of the expressions we present are straight-forward and can be evaluated in the whole physical domain of the problem. First we summarize some previous work where solutions for this problem have been reported, at least ostensibly.

In 2002 [14], Kong provided a thorough analysis of the electromagnetic fields due to a point-source within a planar layered media wherein any particular layer could have a positive or negative relative permittivity and permeability. He considers both 2D and 3D problems and also provides expressions for the special cases of a slab of double-negative material (i.e., the VL). See Section VI-C of his paper for the 2D case of a line-source excitations and Section VII-E for an electric dipole in front of the VL. He leaves all his expressions in terms of spectral-domain representations (see, e.g., equations 190-209 of his paper) and because these integrals represent functions having a singularity making them difficult to compute, there has been much speculation on interpreting the electromagnetics of the VL.

None the less, for the past two decades the use of double negative materials has been investigated for a vast number of applications including super-resolution for nano-scale object imaging, [15]–[17], microwave imaging, [18]–[21], object cloaking and insulating, [22], manufacturing electronic sensors, [23], bio-medicine and biomedical imaging, [24], [25], as well as recent applications such as optical computing [26] and energy harvesting [27]. The concept has even been extended to that of heat conduction, [28].

Our interest lies in the use of a VL for microwave imaging (see, e.g., [18], [20], [21], [29]). The standard procedure would be to use a physical (even if only approximate) VL during the imaging process and then utilizing the focusing nature of the lens to obtain well-conditioned inversion matrices. Even in the theoretical work reported in [20], [21], [29], a small amount of loss was introduced into the Green's function for the VL so as to allow the spectral-domain representations to converge and thereby construct suitable inverse-scattering matrices for the inverse problem. Therefore, there is a clear need for the simplified expressions derived herein which do not require that any loss be introduced.

In this research, to the best of the authors' knowledge, an explicit form of the Green's functions representing electromagnetic fields of both a line-source and a point-source in front of a semi-infinite slab of double-negative material (i.e., the ideal VL) located in the free-space without assuming any loss real or numerical loss or frequency dispersion are derived. The procedure is simply to arrive at solutions that: a) satisfy Maxwell's equations in all domains, b) satisfy appropriate boundary conditions at all boundaries of the problem, and c) explicitly enforce conservation of power. These solutions do contain singularities: the conventional singularity at the point-source plus two additional singularities within the VL and at the focus point, but these are analyzed as "power-transfer singularities" which merely transfer power from the one side of the "power-transfer singularity planes"

1. The infinite extent of the VL already makes it not physically realizeable, but here we allude to the potential requirement for new sources to be created by the VL, violating conservation of charge.

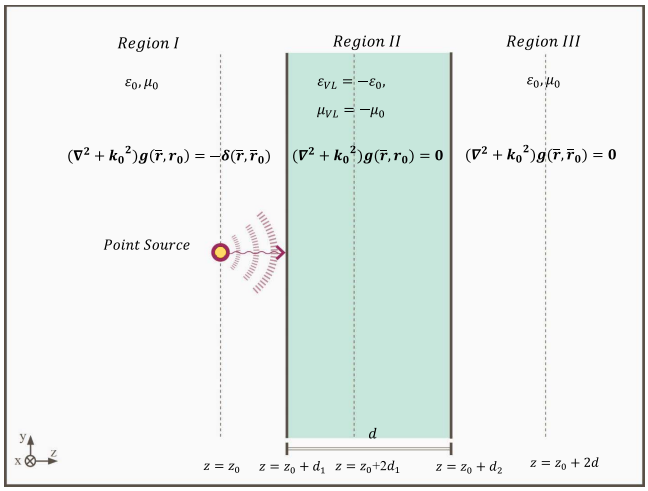

FIGURE 2. Problem statement; a point-source in front of a VL with thickness $d = d_2 - d_1$ in the free-space. The VL boundaries at $z = z_0 + d_1$ and $z = z_0 + d_2$ split the space into the three regions I, II and III for $z - z_0 < d_1$, $d_1 \le z - z_0 \le d_2$, and $z - z_0 > d_2$, respectively. Corresponding to each region a Helmholtz equation along with its associated BCs holds.

to the other (they are not the traditional source or sink singularities). Requirements for boundedness of the solution at these transfer singularities can be accommodated by assuming the sum of the two solutions on either sides of the transfer plane, but, other than boundedness of the solution, there is no physical principal to justify such a construction.

II. THE 2D AND 3D VL GREEN'S FUNCTION

In this section the 2D and 3D Green's functions for the VL are obtained based on expected power flow considerations as well as appropriate boundary conditions (BCs) for the VL. As illustrated in Fig. 2, for the VL we consider a slab of double-negative material with $\epsilon_{VL} = \epsilon_0\epsilon_r$ and $\mu_{VL} = \mu_0\mu_r$, where $\mu_r = -1$ and ϵ_0 and μ_0 are the permittivity and permeability of the free-space. As in the figure the two VL interfaces are located at $z = z_0 + d_1$ and $z = z_0 + d_2$ where d_1 is the distance of the lens from a point-source located on the left hand side of the VL at $\bar{r}_0 = (x_0, y_0, z_0)$, and $d \triangleq d_2 - d_1$ is the thickness of VL. The regions shown in the diagram are defined as the set of all the spatial points $\bar{r} = (x, y, z)$ such that $z - z_0 < d_1$ in Region I, $d_1 \le z - z_0 \le d_2$ in Region II, and $z - z_0 > d_2$ in Region III.

A. GREEN'S FUNCTIONS: PDE SOLUTIONS IN THE FIRST REGION

The electromagnetic problem for the VL configuration shown in Fig. 2 can be formulated in terms of the Helmholtz equation for the magnetic vector potential $\bar{A}$:

$$\nabla^2\bar{A} + k^2\bar{A} = -\mu_0\mu_r\bar{J}, \tag{1}$$

where $k = \omega\sqrt{\mu_0\mu_r\epsilon_0\epsilon_r}$ is the wavenumber. Notice that the relative permittivity and permeabilities are that of free-space to the left and right of the lens and double negatives inside the lens. Once the magnetic vector potential is found, the electric and magnetic fields are obtained as [30]

$$\bar{E} = -j\omega\bar{A} + \frac{1}{j\omega\epsilon_0\epsilon_r\mu_0\mu_r}\nabla(\nabla\cdot\bar{A}), \tag{2a}$$

$$\bar{H} = \frac{1}{\mu_0\mu_r}\nabla\times\bar{A}. \tag{2b}$$

The vectorial nature of the fields depends on the type and orientation of the source located in Region I.

It is essential to note that the wavenumber in all three regions shown in the Fig. 2 is the same. The wavenumber $k = k_0 = \omega\sqrt{\mu_0\epsilon_0}$ in all three regions including the double-negative Region II (the two negative cancel out). The only difference in the partial differential equation (PDE) that needs to be satisfied in each region is the presence or absence of a source.

The 2D point-source problem, corresponding to a 3D line-source, produces fields that are transverse magnetic to the x-axis containing only the E_x, H_y, H_z field components. These can be obtained by solving for the A_x component of the magnetic vector potential satisfying the scalar Helmholtz equation:

$$\left(\nabla^2 + k_0^2\right)A_x(\bar{r}|\bar{r}_0) = \begin{cases} -\mu_0\mu_r J_x(\bar{r}) & \text{Region I} \\ 0 & \text{Regions II, III,} \end{cases} \tag{3}$$

where $J_x(\bar{r}) = I\delta(\bar{r} - \bar{r}_0)$ and $\bar{r} \triangleq (y, z)$ is the 2D position vector.

This is the same PDE as for a 2D scalar Green's function, $g_0(\bar{r}|\bar{r}_0)$ but with right-hand-side given as $-\mu_0\mu_r I\delta(\bar{r} - \bar{r}_0)$, so the magnetic vector potential is just given by $A_x = \mu_0\mu_r I g_0(\bar{r}|\bar{r}_0)$.

For the 3D vector problem

$$(\nabla^2 + k_0^2)\bar{A}(\bar{r}|\bar{r}_0) = \begin{cases} -\mu_0\mu_r\bar{J}(\bar{r}) & \text{Region I} \\ \bar{0} & \text{Regions II, III,} \end{cases} \tag{4}$$

there are two cases depending on the polarization of the point-source. The first case, which we denote as the ZED polarization, assumes that an electric (dipole) point-source is polarized in the z-direction and produces a transverse magnetic, TMz, field to z-direction. The components of this electromagnetic field can be obtained by solving the scalar Helmholtz equation for the A_z component of the magnetic vector potential with source $J_z(\bar{r}) = Il\delta(\bar{r} - \bar{r}_0)$ where $\bar{r} = (x, y, z)$ is the 3D position vector. In this case, the PDE is the same as for a scalar Green's function, $g_0(\bar{r}|\bar{r}_0)$ with right-hand-side given as $-\mu_0\mu_r Il\delta(\bar{r} - \bar{r}_0)$. So the magnetic vector potential is just given by $A_z = \mu_0\mu_r Il g_0(\bar{r}|\bar{r}_0)$. The remaining components of the magnetic vector potential will be zero (by symmetry there is no mixing of components at the boundaries).

The second polarization, denoted YED, is similarly obtained by assuming an electric (dipole) point-source polarized in the y-direction: $J_y(\bar{r}) = Il\delta(\bar{r})$, producing only the y-component of the magnetic vector potential, $A_y = \mu_0\mu_r Il g_0(\bar{r}|\bar{r}_0)$.

The BCs on the scalar Green's function will be different for these two polarizations as will be explained in the next section. The XED polarization can be easily obtained from the YED polarization by a rotation of coordinates and will not be considered herein.

To find the solutions of the 2D and 3D problems in the first region, we require the well-established principle stating that the VL does not reflect any energy from its boundary, [1], [2]. That is, the VL is transparent to electromagnetic fields produced in Region I. In fact this is one of the desirable features of the VL which brought it to prominence. Given these observations we note that for both 2D and 3D problems the field solutions in Region I can be simply obtained from the free-space Green's function.

Recall that the 2D Green's function for the Helmholtz PDE has two solutions:

$$\frac{j}{4}\,H_0^{(1)}(k_0R), \quad \text{and} \quad \frac{-j}{4}\,H_0^{(2)}(k_0R), \tag{5}$$

where $R \triangleq \|\bar{r}-\bar{r}_0\|$ is the distance from the observation point to the point-source and $H_0^{(i)}$ denotes of zeroth-order Hankel function of the i^{th} kind, for $i = 1, 2$. Taking into account the $e^{j\omega t}$ time convention, the $H_0^{(1)}$ solution corresponds to energy flow into the point-source whereas the $H_0^{(2)}$ solution corresponds to energy flow away from the point-source. Clearly then, in Region I we require the $H_0^{(2)}$ solution because we want the power to flow away from the source of energy. In 3D the two solutions are:

$$\frac{e^{jk_0R}}{4\pi R}, \quad \text{and} \quad \frac{e^{-jk_0R}}{4\pi R}, \tag{6}$$

where, again, the first corresponds to incoming waves whereas the second to outgoing waves. Thus, the appropriate Green's function is the latter.

Now that we have the form of the solution in Region I the BCs and power-flow considerations will dictate the solutions in the remaining regions. As will be seen, the BCs will not be sufficient to determine the form of the solution in the entire regions II and III. We will be required to break Regions II and III into two sub-regions based on the expected power flow of the solution in each region. This will be elaborated in Section (II-C).

B. VL BOUNDARY CONDITIONS

The electromagnetic BCs at the surfaces of the VL are the well-known continuity of the tangential electric and magnetic fields, Thus, we have

$$\begin{cases} \hat{n} \times \left(\bar{E}\Big|_{z=z_0+d_n^+} - \bar{E}\Big|_{z=z_0+d_n^-} \right) = \bar{0}, \\ \hat{n} \times \left(\bar{H}\Big|_{z=z_0+d_n^+} - \bar{H}\Big|_{z=z_0+d_n^-} \right) = \bar{0}, \end{cases} \tag{7}$$

where the subscript $n = 1, 2$, and $\hat{n}$ is the unit normal to the boundary. For uniqueness of solutions in an electromagnetic boundary value problem (BVP) we are required to impose only one of these conditions, the other will follow automatically.

1) 2D VL PROBLEM

In the 2D problem, A_x, the magnetic vector potential produces only the E_x component of the electric field via (2a) as

$$\bar{E} \;=\; -j\omega A_x \hat{x} \tag{8}$$

and from (2b), we find

$$\bar{H} \;=\; \tfrac{1}{\mu_0\mu_r}\nabla \times \bar{A} \;=\; \frac{1}{\mu_0\mu_r}\left(\hat{y}\,\frac{\partial A_z}{\partial z} - \hat{z}\,\frac{\partial A_z}{\partial y} \right). \tag{9}$$

The continuity of the electric field across the boundaries leads to the continuity A_x, while the second condition in (7), gives rise that

$$\frac{1}{\mu_r}\,\frac{\partial A_x}{\partial z}\Big|_{z=z_0+d_n^-} = \frac{1}{\mu_r}\,\frac{\partial A_x}{\partial z}\Big|_{z=z_0+d_n^+}, \tag{10}$$

for $n = 1, 2$. Noting that over both boundaries, $z = z_0 + d_1$ and $z = z_0 + d_2$, the relative permeability changes its sign, the BCs (7) for A_x become

$$\begin{cases} A_x\Big|_{z=z_0+d_n^-} = A_x\Big|_{z=z_0+d_n^+}, \\ \frac{\partial A_z}{\partial z}\Big|_{z=z_0+d_n^-} = -\,\frac{\partial A_z}{\partial z}\Big|_{z=z_0+d_n^+} \end{cases} \tag{11}$$

for $n = 1, 2$.

Recalling that $A_x = \mu_0\mu_r I g_0(\bar{r}|\bar{r}_0)$, the complete scalar 2D BVP can be written as

$$\begin{cases} (\nabla^2 + k_0^2) g_0(\bar{r}|\bar{r}_0) \;=\; -\,\delta(\bar{r}-\bar{r}_0), & z - z_0 \le d_1, \\ (\nabla^2 + k_0^2) g_0(\bar{r}|\bar{r}_0) \;=\; 0, & d_1 \le z - z_0 \le d_2, \\ (\nabla^2 + k_0^2) g_0(\bar{r}|\bar{r}_0) \;=\; 0, & z - z_0 \ge d_2, \end{cases} \tag{12}$$

with the following BCs

$$\begin{cases} g_0(\bar{r}|\bar{r}_0)\Big|_{z=z_0+d_n^-} = -g_0(\bar{r}|\bar{r}_0)\Big|_{z=z_0+d_n^+}, \\ \frac{\partial g_0(\bar{r}|\bar{r}_0)}{\partial z}\Big|_{z=z_0+d_n^-} = \frac{\partial g_0(\bar{r}|\bar{r}_0)}{\partial z}\Big|_{z=z_0+d_n^+}, \end{cases} \tag{13}$$

for $n = 1, 2$. It will be shown that the first condition is sufficient to obtain a solution in all regions.

2) 3D VL PROBLEM

The same BCs, (7), apply to the 3D problem. How these transfer to the scalar Green's function needs to be checked for both the ZED and YED polarizations. Recall that for the ZED polarization the z-component of the magnetic vector potential, A_z, satisfies (4). The fields are then obtained using 2a and 2b, giving

$$\bar{E} = -j\omega\Big\{ \hat{z}A_z + \frac{1}{k_0^2}\left[\hat{x}\,\frac{\partial^2 A_z}{\partial x \partial z} + \hat{y}\,\frac{\partial^2 A_z}{\partial y \partial z} + \hat{z}\,\frac{\partial^2 A_z}{\partial z^2} \right] \Big\}. \tag{14}$$

and

$$\bar{H} = \frac{1}{\mu_0\mu_r}\left(\hat{x}\,\frac{\partial A_z}{\partial y} - \hat{y}\,\frac{\partial A_z}{\partial x} \right). \tag{15}$$

This results in the following BCs for the magnetic vector potential

$$\begin{cases} \left.\frac{\partial A_z}{\partial x}\right|_{z=z_0+d_n^-} = -\left.\frac{\partial A_z}{\partial x}\right|_{z=z_0+d_n^+}, \\ \left.\frac{\partial A_z}{\partial y}\right|_{z=z_0+d_n^-} = -\left.\frac{\partial A_z}{\partial y}\right|_{z=z_0+d_n^+}, \end{cases} \tag{16}$$

for $n = 1, 2$.

Recalling that $A_z = \mu_0\mu_r Il g_0(\bar{r}|\bar{r}_0)$, we may conclude that the 3D BVP (for the ZED polarization) for the 3D scalar function $g_0(\bar{r}|\bar{r}_0)$ should satisfy

$$\begin{cases} (\nabla^2 + k_0^2) g_0(\bar{r}|\bar{r}_0) &= -\delta(\bar{r} - \bar{r}_0), & z - z_0 \le d_1, \\ (\nabla^2 + k_0^2) g_0(\bar{r}|\bar{r}_0) &= 0, & d_1 \le z - z_0 \le d_2, \\ (\nabla^2 + k_0^2) g_0(\bar{r}|\bar{r}_0) &= 0, & z - z_0 \ge d_2, \end{cases} \tag{17}$$

with the following BCs

$$\begin{cases} \left.\frac{\partial g_0(\bar{r}|\bar{r}_0)}{\partial x}\right|_{z=z_0+d_n^-} = \left.\frac{\partial g_0(\bar{r}|\bar{r}_0)}{\partial x}\right|_{z=z_0+d_n^+}, \\ \left.\frac{\partial g_0(\bar{r}|\bar{r}_0)}{\partial y}\right|_{z=z_0+d_n^-} = \left.\frac{\partial g_0(\bar{r}|\bar{r}_0)}{\partial y}\right|_{z=z_0+d_n^+}, \end{cases} \tag{18}$$

for $n = 1, 2$.

Next, for a YED polarization the y-component of $\bar{A}$ satisfies (4). Using 2a and 2b, the fields are obtained as

$$\bar{E} = -j\omega\Big\{\hat{y}A_y + \frac{1}{k_0^2}\left[\hat{x}\,\frac{\partial^2 A_y}{\partial x \partial y} + \hat{y}\,\frac{\partial^2 A_y}{\partial y^2} + \hat{z}\,\frac{\partial^2 A_y}{\partial z \partial y}\right]\Big\}. \tag{19}$$

and

$$\bar{H} = \frac{1}{\mu_0\mu_r}\left(-\hat{x}\,\frac{\partial A_y}{\partial z} + \hat{z}\,\frac{\partial A_y}{\partial x}\right) \tag{20}$$

resulting in the BCs

$$\begin{cases} A_y\Big|_{z=z_0+d_n^-} = A_y\Big|_{z=z_0+d_n^+}, \\ \left.\frac{\partial A_y}{\partial z}\right|_{z=z_0+d_n^-} = -\left.\frac{\partial A_y}{\partial z}\right|_{z=z_0+d_n^+} \end{cases} \tag{21}$$

for $n = 1, 2$. Recalling that $A_y = \mu_0\mu_r Il g_0(\bar{r}|\bar{r}_0)$, the following BCs should be considered for the YED polarization

$$\begin{cases} g_0(\bar{r}|\bar{r}_0)\Big|_{z=z_0+d_n^-} = -g_0(\bar{r}|\bar{r}_0)\Big|_{z=z_0+d_n^+}, \\ \left.\frac{\partial g_0(\bar{r}|\bar{r}_0)}{\partial z}\right|_{z=z_0+d_n^-} = \left.\frac{\partial g(\bar{r}|\bar{r}_0)}{\partial z}\right|_{z=z_0+d_n^+}, \end{cases} \tag{22}$$

for $n = 1, 2$. The PDE of the BVP will be the same as in the ZED case.

C. VL GREEN'S FUNCTION; POWER FLOW AND THE SOLUTIONS IN THE SECOND AND THIRD REGIONS

In Section (II-A), we chose the proper 2D and 3D solutions for Region I which satisfies the Helmholtz PDE in that region. In this section, we choose solutions in Regions II and III that satisfy the homogeneous Helmholtz equations as well as the BCs given in the BVPs. The form of the solutions dictated by the BCs results in singularities arising within these regions which will be dealt with using power flow considerations.

1) 2D VL PROBLEM

Recall that based on the expected direction of power flow from the x-directed line-source in the 2D case, we have chosen the solution in Region I as the second solution in (5). Clearly, the BC at the first boundary, requires that the solution be of the same form but with the opposite sign to the right of the boundary as to the left. Considering the 2D case first, we define a point $\bar{r}_1 \triangleq (y_0, z_0 + 2d_1)$ located inside the VL and form the solution as

$$\frac{j}{4}\,H_0^{(2)}(k_0 R_1), \quad d_1 \le z \le 2d_1 \tag{23}$$

where $R_1 \triangleq \|\bar{r} - \bar{r}_1\|$ is the distance from any point $\bar{r} = (y, z)$ inside Region II. It will be checked subsequently that the fields obtained from this solution satisfy the necessary BC that the tangential electric and magnetic fields are continuous.

We have restricted this solution to Region II-A defined as $d_1 \le z \le 2d_1$ because although this solution obviously satisfies the BC, it creates a singular point at $\bar{r}_1 = (y_0, z_0 + 2d_1)$ located inside the VL. This singularity has been the source of much discussion in the literature [2], [9], [31]–[33]. We can therefore say that we only have the appropriate solution in Region II-A. Ignoring the singularity for the moment, we note that this form of the solution represents power flow away from the boundary toward the singularity (the double negative material reverses the normal solution that represents outward power flow in a regular medium). The power flow is conserved across the boundary and "accumulates" at the singularity. As will be shown later, no power crosses the regular part of the surface $z = z_0 + 2d_1$. Thus, to satisfy conservation of power the solution to the right of this surface, Region II-B, must be of the form

$$\frac{j}{4}\,H_0^{(1)}(k_0 R_1), \quad 2d_1 < z - z_0 \le d_2, \tag{24}$$

The magnitude of the coefficient ensures that the power is conserved across the singularity but we obviously could have taken the negative of this solution obtained the same conservation. There are two physical principles that can be put into play to justify the coefficient chosen. Firstly, the negative of this solution would result in a flipping of the polarization and there is no expectation that the fields within the VL would undergo such a flip. Secondly, the reader may have noticed that the imaginary parts of the solutions (23) and (24) on both sides of the surface $z = z_0 + 2d$ are complex conjugates of each other (i.e., $H_0^{(1)} = J_0 + jY_0$ and $H_0^{(2)} = J_0 - jY_0$), thus, to enforce boundedness of the solution at the singularity one could assume that on the $z = z_0 + 2d_1$ the solution is simply the sum of the two solutions, $j/2J_0(k_0R_1)$.

Turning our attention to Region III, firstly we define the point $\bar{r}_2 = (y_0, z_0 + 2d)$ and restrict the solution into the sub-region III-A located between the surfaces $z = z_0 + d_2$ and $z = z_0 + 2d$. Then applying the required BCs on both sides of $z = z_0 + d_2$ obviously dictates us to choose the same form of the solution with the opposite sign as in Region II-B

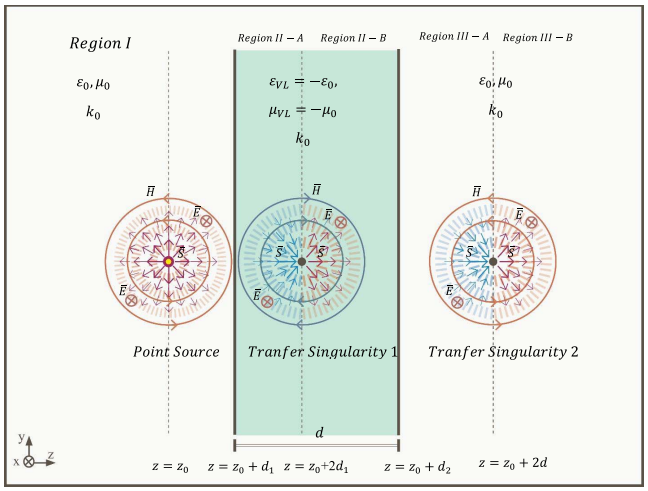

FIGURE 3. Power flow of an *x*-directed line-source; the outgoing and incoming power flows in the five different sub-regions show that the VL phenomena creates two singularities with different physical properties than a source or a sink.

for the Region III-A as

$$\frac{-j}{4} H_0^{(1)}(k_0 R_2), \quad d_2 \le z - z_0 < 2d, \tag{25}$$

where $R_2 = \|\bar{r} - \bar{r}_2\|$ is the distance from any point $\bar{r} = (y, z)$ inside Region III. Note that the solution is capable of producing incoming power flow and accumulating the power into the second singularity. Using a similar interpretation we used in Region II, to choose the appropriate solution for the remaining half-space after the surface $z = z_0 + 2d$, called Region III-B, we note that while the solution should satisfy the conservation of power, it should also produce an outgoing power flow. Hence, this leads us to choose the solution

$$\frac{-j}{4} H_0^{(2)}(k_0 R_2), \quad z - z_0 > 2d \tag{26}$$

in Region III-B. Similarly, to justify the sign we have chosen for the solution (26), we should note to the two physical principles, which we applied to find the sign of the solution in region II-B; the expected polarization as well as boundedness of the solution. So, to achieve a bounded solution along the surface $z = z_0 + 2d$, one may assume, $j/2J_0(k_0 R_2)$ obtained as the sum of the two solutions on both sides.

The required power flow as well as the direction of the electromagnetic fields for an *x*-directed line-source in the five different regions are depicted in Fig. (3).

2) 3D VL PROBLEM

The procedure for finding the Green's functions for the different polarizations in 3D is similar to the procedure just described in 2D. The form of the Green's function in Region I has already been chosen as the latter of (6). For the ZED source the BCs have already been determined as in (18). The BC at the first boundary of the VL requires us to choose a solution of the same form and with the same sign on the right side of the boundary as on the left. Thus, the solution in sub-region II-A, between the surfaces $z = z_0 + d_1$ and $z = z_0 + 2d_1$, is written as

$$\frac{e^{-jk_0 R_1}}{4\pi R_1}, \quad d_1 \le z - z_0 < 2d_1, \tag{27}$$

where $R_1 = \|\bar{r} - \bar{r}_1\|$ is the distance from any point $\bar{r} = (x, y, z)$ inside Region II to the interior singular point $\bar{r}_1 \triangleq (x_0, y_0, z_0 + 2d_1)$ located inside the VL. As in the 2D case, it will be observed that the power flow represented by this solution is an incoming power flow away from the boundary in sub-region II-A and accumulating at the interior singular point. Again, following a similar logic applied in the 2D problem, in order to satisfy conservation of power, in sub-region II-B we must choose the solution as

$$\frac{e^{jk_0 R_1}}{4\pi R_1}, \quad 2d_1 < z - z_0 \le d_2. \tag{28}$$

The polarity of the coefficient was again chosen to take into account the two principles that there should be no flipping of the polarization through the singularity and the boundedness of the fields at the singularity. The boundedness can be preserved by assuming that on the $z = z_0 + 2d_1$ plane we have the sum of the two solutions giving us the finite solution $\cos(k_0 R_1)/2\pi R_1$ on this plane.

Enforcing the second BC at $z = z_0 + d_2$ and following a similar approach explained to find the solutions in Region II, leads to the solution

$$\frac{e^{jk_0 R_2}}{4\pi R_2}, \quad d_2 < z - z_0 \le 2d, \tag{29}$$

in Region III-A, and

$$\frac{e^{-jk_0 R_2}}{4\pi R_2}, \quad z - z_0 \ge 2d \tag{30}$$

in Region III-B where $R_2 = \|\bar{r} - \bar{r}_2\|$ is the distance from any point $\bar{r} = (x, y, z)$ inside Region III to the second singular point $\bar{r}_2 \triangleq (x_0, y_0, z_0 + 2d)$ located outside the VL on the opposite side of the VL from where point-source is located. As before, the solutions in sub-regions III-A and III-B are conjugates of each other and we may again assume the finite solution $\cos(k_0 R_2)/2\pi R_2$ on the plane $z = z_0 + 2d$.

D. SUMMARY OF GREEN'S FUNCTIONS AND INTERPRETATION

Summarizing the 2D solutions in the (y, z)-plane for a VL of thickness d and electric point-source located at $\bar{r}_0$ a distance d_1 from its surface we have:

$$g_0(\bar{r}|\bar{r}_0, d_1, d) = \begin{cases} \frac{-j}{4} H_0^{(2)}(k_0 R), & z - z_0 \le d_1 \\ \frac{j}{4} H_0^{(2)}(k_0 R_1), & d_1 \le z - z_0 < 2d_1 \\ \frac{j}{4} H_0^{(1)}(k_0 R_1), & 2d_1 < z - z_0 \le d_2 \\ \frac{-j}{4} H_0^{(1)}(k_0 R_2), & d_2 \le z - z_0 < 2d \\ \frac{-j}{4} H_0^{(2)}(k_0 R_2), & z - z_0 > 2d, \end{cases} \tag{31}$$

where $R_1 = \|\bar{r} - \bar{r}_1\|$, $R_2 = \|\bar{r} - \bar{r}_2\|$, $\bar{r}_1 = (y_0, z_0 + 2d_1)$, and $\bar{r}_2 = (y_0, z_0 + 2d)$.

The Green's function for the 3D ZED polarization is:

$$g_0(\bar{r}|\bar{r}_0,d_1,d)=\begin{cases}\frac{e^{-jk_0R}}{4\pi R}, & z-z_0\le d_1\\ \frac{e^{-jk_0R_1}}{4\pi R_1}, & d_1\le z-z_0<2d_1\\ \frac{e^{jk_0R_1}}{4\pi R_1}, & 2d_1<z-z_0\le d_2\\ \frac{e^{jk_0R_2}}{4\pi R_2}, & d_2\le z-z_0<2d\\ \frac{e^{-jk_0R_2}}{4\pi R_2}, & z-z_0>2d,\end{cases}\quad(32)$$

wherein $R_1=\|\bar{r}-\bar{r}_1\|$, $R_2=\|\bar{r}-\bar{r}_2\|$, $\bar{r}_1=(x_0,y_0,z_0+2d_1)$ and $\bar{r}_2=(x_0,y_0,z_0+2d)$.

Similarly, the 3D YED Green's function is

$$g_0(\bar{r}|\bar{r}_0,d_1,d)=\begin{cases}\frac{e^{-jk_0R}}{4\pi R}, & z-z_0\le d_1\\ -\frac{e^{-jk_0R_1}}{4\pi R_1}, & d_1\le z-z_0<2d_1\\ -\frac{e^{jk_0R_1}}{4\pi R_1}, & 2d_1<z-z_0\le d_2\\ \frac{e^{jk_0R_2}}{4\pi R_2}, & d_2\le z-z_0<2d\\ \frac{e^{-jk_0R_2}}{4\pi R_2}, & z-z_0>2d,\end{cases}\quad(33)$$

As can be clearly seen, these Green's functions are not continuous across the VL boundaries but they do produce continuous tangential electric and magnetic fields across the VL boundaries. In addition they result in singularities at two points: $\bar{r}_1=0$ and $\bar{r}_2=0$ both in 2D and 3D. As has already been described these singularities are not sources or sinks of energy and therefore not the traditional singularities arising in physics but a new kind of singularity that we now refer to as a power-transfer singularity because power enters from one side and exits from the other. This is depicted in Fig. (3). These singularities exist on power-transfer planes, $z=z_0+2d_1$ and $z=z_0+2d$ across which there is no power flow (except for at the transfer singularities). As will be shown in the next two sections where expressions for the electromagnetic fields and the Poynting vector are given, some of the components of the electromagnetic field are discontinuous across the transfer planes. We don't consider the discontinuities of the tangential components of the field problematic as there is no power flow across these planes. As will be seen, we also obtain a discontinuity in the normal component of the electric flux density which does have some implications for the physical realizability of the ideal VL.

Finally, the issue of non-causal solutions is eliminated because the power flow is away from the point-source and in the physically correct direction on either side of the transfer plane. We believe this completely resolves earlier concerns regarding violation of physical rules based on viewing the solutions as composed of backward-traveling waves [34]. Our solutions have been derived for the lossless VL without the need for assuming an infinitesimal loss nor frequency dispersion in the problem, [35].

III. ELECTROMAGNETIC FIELDS AND POYNTING VECTOR

In this section we provide explicit expressions for the electromagnetic fields as well as for the Poynting vector in all regions of the VL. To simplify notation we now assume the point-source to be located at the origin, $\bar{r}_0=0$. Thus, for the x-directed line-source with current $J_x(\bar{r})=I\delta(\bar{r})$ producing a magnetic vector potential, $\bar{A}=A_x\hat{x}$ the fields can be obtained by relations (8) and (9). So, noting that $A_x=\mu_0\mu_r I g_0(\bar{r}|\bar{r}_0)$, using the 2D scalar Green's function introduced in (31), it is easy to find the fields as

$$\bar{E}(\bar{r}|d_1,d)=-\frac{\omega\,\mu_0 I}{4}\,\hat{x}\begin{cases}H_0^{(2)}(k_0r), & z\le d_1\\ H_0^{(2)}(k_0r_1), & d_1\le z<2d_1\\ H_0^{(1)}(k_0r_1), & 2d_1<z\le d_2\\ H_0^{(1)}(k_0r_2), & d_2\le z<2d\\ H_0^{(2)}(k_0r_2), & z>2d,\end{cases}\quad(34)$$

and

$$\bar{H}(\bar{r}|d_1,d)=\frac{jk_0 I}{4}\begin{cases}H_0^{(2)}(k_0r)\hat{\theta}, & z\le d_1\\ -H_0^{(2)}(k_0r_1)\hat{\theta}_1, & d_1\le z<2d_1\\ -H_0^{(1)}(k_0r_1)\hat{\theta}_1, & 2d_1<z\le d_2\\ H_0^{(1)}(k_0r_2)\hat{\theta}_2, & d_2\le z<2d\\ H_0^{(2)}(k_0r_2)\hat{\theta}_2, & z>2d,\end{cases}\quad(35)$$

where now $R=\|\bar{r}\|=r$, $R_1=\|\bar{r}_1\|=r_1$, and $R_2=\|\bar{r}_2\|=r_2$ and $\hat{\theta}=\frac{z\hat{y}-y\hat{z}}{\sqrt{y^2+z^2}}$, $\hat{\theta}_1=\frac{(z-2d_1)\hat{y}-y\hat{z}}{\sqrt{y^2+(z-2d_1)^2}}$ and $\hat{\theta}_2=\frac{(z-2d)\hat{y}-y\hat{z}}{\sqrt{y^2+(z-2d)^2}}$.

Plots of the electric field corresponding to (34) as well as observations regarding its value at the particular boundaries of interest are provided in Section III-A.

Next, the Poynting vector can be found as

$$\begin{aligned}\bar{S}(\bar{r}|d_1,d)&=\bar{E}(\bar{r}|d_1,d)\times\bar{H}^*(\bar{r}|d_1,d)\\&=\eta\left[\frac{k_0I}{4\pi}\right]^2\begin{cases}C(k_0\bar{r})\,\hat{r}, & z\le d_1\\ -C(k_0\bar{r}_1)\,\hat{r}_1, & d_1\le z<2d_1\\ C^*(k_0\bar{r}_1)\,\hat{r}_1, & 2d_1<z\le d_2\\ -C^*(k_0\bar{r}_2)\,\hat{r}_2, & d_2\le z<2d\\ C(k_0\bar{r}_2)\,\hat{r}_2, & z>2d,\end{cases}\end{aligned}\quad(36)$$

where $\hat{r}=\frac{y\hat{y}+z\hat{z}}{\sqrt{y^2+z^2}}$, $\hat{r}_1=\frac{y\hat{y}+(z-2d_1)\hat{z}}{\sqrt{y^2+(z-2d_1)^2}}$ and $\hat{r}_2=\frac{y\hat{y}+(z-2d)\hat{z}}{\sqrt{y^2+(z-2d)^2}}$. Also, $C^*(\cdot)$ indicates the complex conjugate of $C(\cdot)\triangleq[J_1(\cdot)Y_0(\cdot)-J_0(\cdot)Y_1(\cdot)]+j[J_0(\cdot)J_1(\cdot)]$, and J_ν and Y_ν are respectively the Bessel functions of ν^{th} order for $\nu=0,1$.

Using identity (D-17) on [30, p. 463], the time-average Poynting power density can be obtained from (36) as

$$\begin{aligned}\langle\bar{S}(\bar{r}|d_1,d)\rangle&=\frac{1}{2}\Re\{\bar{S}(\bar{r}|d_1,d)\}\\&=\frac{\eta}{\pi}\left[\frac{k_0I}{4}\right]^2\begin{cases}\frac{1}{r}\hat{r}, & z\le d_1\\ -\frac{1}{r_1}\hat{r}_1, & d_1\le z<2d_1\\ \frac{1}{r_1}\hat{r}_1, & 2d_1<z\le d_2\\ -\frac{1}{r_2}\hat{r}_2, & d_2\le z<2d\\ \frac{1}{r_2}\hat{r}_2, & z>2d,\end{cases}\end{aligned}\quad(37)$$

where $\Re$ indicates the real part of a complex number.

As can be observed from these expressions for the power density, the amount of incoming power at the singularities of Regions II and III are equal to that of outgoing power from these same singularities. Also, at the transfer planes the power flow is tangent to the plane with no vectorial component crossing the plane. This is indicated in Fig. (3) by the color of the arrows representing $\bar{S}$.

The 3D electromagnetic fields for the different polarizations can also be easily obtained as follows. For the ZED polarization, where the source is $\bar{J}(\bar{r}) = \hat{z}Il\delta(\bar{r})$, we have $A_z = \mu_0\mu_r Il\, g_0(\bar{r}|\bar{r}_0)$. So using relation (2a) the electric field can be written as

$$\begin{aligned}\bar{E}(\bar{r}|d_1,d) &= -j\omega\mu_0\mu_r Il\left[1+\frac{1}{k_0^2}\nabla\nabla\right]\cdot\ g_0(\bar{r}|\bar{r}_0,d_1,d)\hat{z}\\ &= -j\omega\mu_0\mu_r Il\left[\hat{z}+\frac{1}{k_0^2}\nabla\frac{\partial}{\partial z}\right]g_0(\bar{r}|\bar{r}_0,d_1,d),\end{aligned} \tag{38}$$

where $\mu_r = -1$ inside the VL and 1 everywhere else and $r = \|\bar{r}\|$, $r_1 = \|\bar{r}_1\| = \|(x,y,z-2d_1)\|$ and $\bar{r}_2 = \|\bar{r}_2\| = \|(x,y,z-2d)\|$, respectively. Thus, in each region the electric field can be written as

$$\bar{E}(\bar{r},d_1,d) = \frac{-j\omega\mu_0 Il}{4\pi}\begin{cases}\left\{\hat{z}\frac{1}{r}\alpha(r)-\frac{z}{r^3}\beta(r)\bar{r}\right\}e^{-jk_0r}, & z\le d_1\\ -\left\{\hat{z}\frac{1}{r_1}\alpha(r_1)-\frac{(z-2d_1)}{r_1^3}\beta(r_1)\bar{r}_1\right\}e^{-jk_0r_1}, & d_1\le z<2d_1\\ -\left\{\hat{z}\frac{1}{r_1}\alpha^*(r_1)-\frac{(z-2d_1)}{r_1^3}\beta^*(r_1)\bar{r}_1\right\}e^{jk_0r_1}, & 2d_1<z\le d_2\\ \left\{\hat{z}\frac{1}{r_2}\alpha^*(r_2)-\frac{(z-2d)}{r_2^3}\beta^*(r_2)\bar{r}_2\right\}e^{jk_0r_2}, & d_2\le z<2d\\ \left\{\hat{z}\frac{1}{r_2}\alpha(r_2)-\frac{(z-2d)}{r_2^3}\beta(r_2)\bar{r}_2\right\}e^{-jk_0r_2}, & z>2d,\end{cases} \tag{39}$$

where

$$\begin{aligned}\alpha(r) &= 1-\frac{j}{k_0r}+\left(\frac{j}{k_0r}\right)^2,\ \text{and}\\ \beta(r) &= 3\alpha(r)-2 = 1-3\frac{j}{k_0r}+3\left(\frac{j}{k_0r}\right)^2,\end{aligned} \tag{40}$$

and α^* and β^* indicate complex conjugates of α and β, respectively. Equivalently, using the cylindrical coordinate unit vectors with $\hat{\rho} = \frac{\hat{x}x+\hat{y}y}{\rho}$ and $\rho = \sqrt{x^2+y^2}$, these can be written as

$$\bar{E}(\bar{r}|d_1,d) = \frac{-j\omega\mu_0 Il}{4\pi}\begin{cases}\left\{\hat{z}\left[\alpha(r)-\frac{z^2}{r^2}\beta(r)\right]\right.\\ \quad\left.-\hat{\rho}\frac{z\rho}{r^2}\beta(r)\right\}\frac{e^{-jk_0r}}{r}, & z\le d_1\\ -\left\{\hat{z}\left[\alpha(r_1)-\frac{(z-2d_1)^2}{r_1^2}\beta(r_1)\right]\right.\\ \quad\left.-\hat{\rho}\frac{(z-2d_1)\rho}{r_1^2}\beta(r_1)\right\}\frac{e^{-jk_0r_1}}{r_1}, & d_1\le z<2d_1\\ -\left\{\hat{z}\left[\alpha^*(r_1)-\frac{(z-2d_1)^2}{r_1^2}\beta^*(r_1)\right]\right.\\ \quad\left.-\hat{\rho}\frac{(z-2d_1)\rho}{r_1^2}\beta^*(r_1)\right\}\frac{e^{jk_0r_1}}{r_1}, & 2d_1<z\le d_2\\ \left\{\hat{z}\left[\alpha^*(r_2)-\frac{(z-2d)^2}{r_2^2}\beta^*(r_2)\right]\right.\\ \quad\left.-\hat{\rho}\frac{(z-2d)\rho}{r_2^2}\beta^*(r_2)\right\}\frac{e^{jk_0r_2}}{r_2}, & d_2\le z<2d\\ \left\{\hat{z}\left[\alpha(r_2)-\frac{(z-2d)^2}{r_2^2}\beta(r_2)\right]\right.\\ \quad\left.-\hat{\rho}\frac{(z-2d)\rho}{r_2^2}\beta(r_2)\right\}\frac{e^{-jk_0r_2}}{r_2}, & z>2d,\end{cases} \tag{41}$$

and completely in spherical coordinates as

$$\bar{E}(\bar{r}|d_1,d) = \frac{-j\omega\mu_0 Il}{4\pi}\begin{cases}\left\{\hat{r}\,[\alpha-\beta](r)\cos\theta\right.\\ \quad\left.-\hat{\theta}\,\alpha(r)\sin\theta\right\}\frac{e^{-jk_0r}}{r}, & z\le d_1\\ -\left\{\hat{r}_1[\alpha-\beta](r_1)\cos\theta_1\right.\\ \quad\left.-\hat{\theta}_1\alpha(r_1)\sin\theta_1\right\}\frac{e^{-jk_0r_1}}{r_1}, & d_1\le z<2d_1\\ -\left\{\hat{r}_1[\alpha-\beta]^*(r_1)\cos\theta_1\right.\\ \quad\left.-\hat{\theta}_1\alpha^*(r_1)\sin\theta_1\right\}\frac{e^{jk_0r_1}}{r_1}, & 2d_1<z\le d_2\\ \left\{\hat{r}_2[\alpha-\beta]^*(r_2)\cos\theta_2\right.\\ \quad\left.-\hat{\theta}_2\alpha^*(r_2)\sin\theta_2\right\}\frac{e^{jk_0r_2}}{r_2}, & d_2\le z<2d\\ \left\{\hat{r}_2[\alpha-\beta](r_2)\cos\theta_2\right.\\ \quad\left.-\hat{\theta}_2\alpha(r_2)\sin\theta_2\right\}\frac{e^{-jk_0r_2}}{r_2}, & z>2d,\end{cases} \tag{42}$$

where

$$\begin{aligned}[\alpha-\beta](r) &= \alpha(r)-\beta(r) = 2(1-\alpha(r))\\ &= 2\left(\frac{j}{k_0r}-\left[\frac{j}{k_0r}\right]^2\right),\\ [\alpha-\beta]^*(r) &= \alpha^*(r)-\beta^*(r) = 2(1-\alpha^*(r))\\ &= -2\left(\frac{j}{k_0r}+\left[\frac{j}{k_0r}\right]^2\right).\end{aligned} \tag{43}$$

Note that to obtain equation (42), similar to the conventional relation $\hat{z} = \hat{r}\cos\theta - \hat{\theta}\sin\theta$ for $z = r\cos\theta$, we have introduced the relations $\hat{z} = \hat{r}_1\cos\theta_1 - \hat{\theta}_1\sin\theta_1$ for $z-2d_1 = r_1\cos\theta_1$ and $\hat{z} = \hat{r}_2\cos\theta_2 - \hat{\theta}_1\sin\theta_1$ for $z-2d = r_2\cos\theta_2$, with shifted spherical coordinate variables and unit vectors as in Fig. 4(b).

The magnetic field for this polarization is written as

$$\bar{H}(\bar{r}|d_1,d) = \frac{1}{-j\omega\mu_0\mu_r}\nabla\times\bar{E}(\bar{r},d_1,d)$$

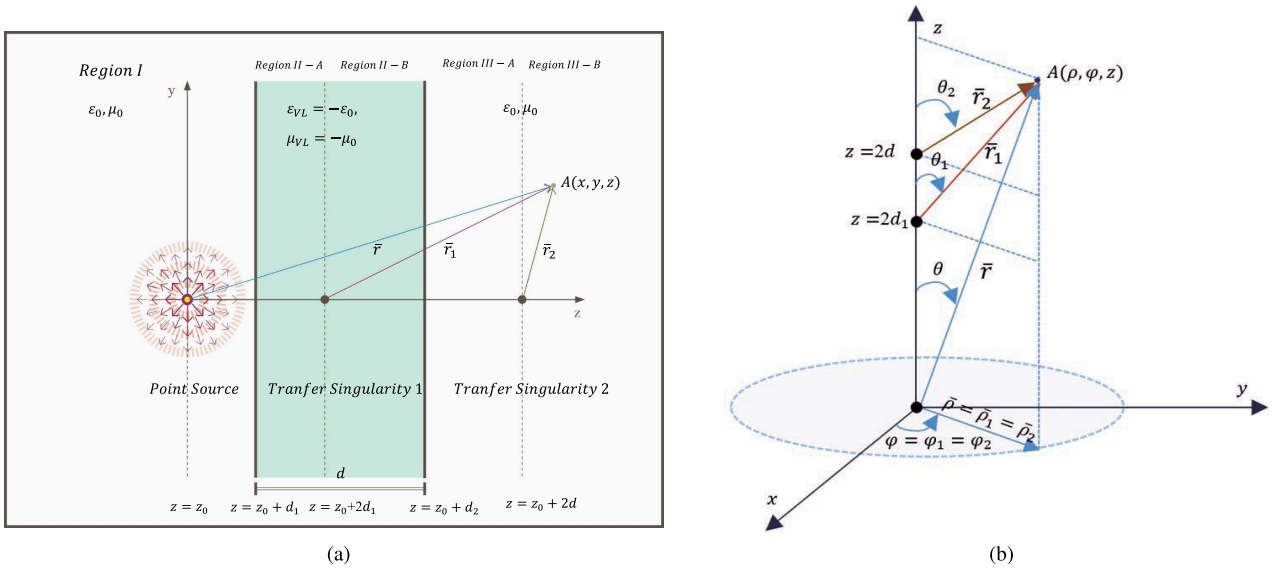

(a) (b)

FIGURE 4. (a) The vectors $\bar{r}$, $\bar{r}_1$ and $\bar{r}_2$ for an arbitrary point A = (*x, y, z*). (b) Representation of the point *A* in different systems of coordinates including cylindrical and spherical coordinates with respect to the three origins located at (0, 0, 0), (0, 0, $2d_1$) and (0, 0, 2d).

$$= \frac{Il}{4\pi} \begin{cases} \left\{ \frac{1}{r^2} \gamma(r) \left(\hat{x}y - \hat{y}x \right) \right\} e^{-jk_0 r}, & z \le d_1 \\ \left\{ \frac{1}{r_1^2} \gamma(r_1) \left(\hat{x}y - \hat{y}x \right) \right\} e^{-jk_0 r_1}, & d_1 \le z < 2d_1 \\ \left\{ \frac{1}{r_1^2} \gamma^*(r_1) \left(\hat{x}y - \hat{y}x \right) \right\} e^{jk_0 r_1}, & 2d_1 < z \le d_2 \\ \left\{ \frac{1}{r_2^2} \gamma^*(r_2) \left(\hat{x}y - \hat{y}x \right) \right\} e^{jk_0 r_2}, & d_2 \le z < 2d \\ \left\{ \frac{1}{r_2^2} \gamma(r_2) \left(\hat{x}y - \hat{y}x \right) \right\} e^{-jk_0 r_2}, & z > 2d, \end{cases} \tag{44}$$

where

$$\gamma(r) = -jk_0 \left(1 - \frac{j}{k_0 r} \right). \tag{45}$$

Equivalently, this can be written in spherical coordinates as

$$\bar{H}(\bar{r}|d_1, d) = \\ = -\hat{\phi}\, Il 4\pi \begin{cases} \gamma(r) \sin\theta \, \frac{e^{-jk_0 r}}{r}, & z \le d_1 \\ \gamma(r_1) \sin\theta_1 \, \frac{e^{-jk_0 r_1}}{r_1}, & d_1 \le z < 2d_1 \\ \gamma^*(r_1) \sin\theta_1 \, \frac{e^{jk_0 r_1}}{r_1}, & 2d_1 < z \le d_2 \\ \gamma^*(r_2) \sin\theta_2 \, \frac{e^{jk_0 r_2}}{r_2}, & d_2 \le z < 2d \\ \gamma(r_2) \sin\theta_2 \, \frac{e^{-jk_0 r_2}}{r_2}, & z > 2d \end{cases} \tag{46}$$

where $\hat{\phi} = \frac{1}{\rho}(-\hat{x}y + \hat{y}x)$. (See Fig. (4(a)) and (4(b)) for the geometric visualization of the applied coordinates in different systems.)

As can be seen from (39) and (44) or (46), the required BCs that the tangential components of electric and magnetic fields be continuous at the VL boundaries are satisfied. It is also apparent that all the field components on one side of the power transfer plane are complex conjugates of the corresponding field components on the other side of the plane. This does not seem to be problematic for the tangential components, but we notice that the electric field is normal to the plane and, thus, also the electric flux density will have such a discontinuity. This discontinuity results in the appearance of a surface charge density on this plane. This is indeed a surprising result that needs to be explained if the ideal VL is physically realizable. Given that there is no conductivity present in the lens, it is unclear exactly how such a surface charge might arise in reality. Alternatively, the complex-conjugate jump across the power transfer plane will need to be interpreted without postulating a supporting surface charge density.

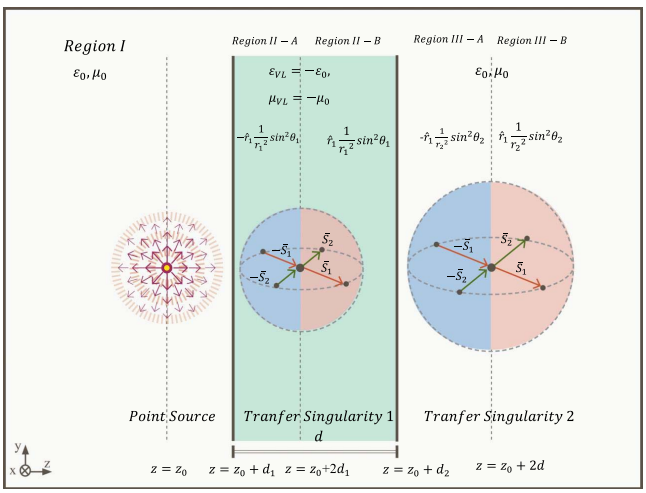

FIGURE 5. The amount of power flowing into the either of the singularities in one side is equal to that of which flowing out from the other side.

Figures (6) and (7) provide plots of the electric fields in the relevant regions. It is worthy to note that our 2D expressions will result in the exact same numerical evaluation of

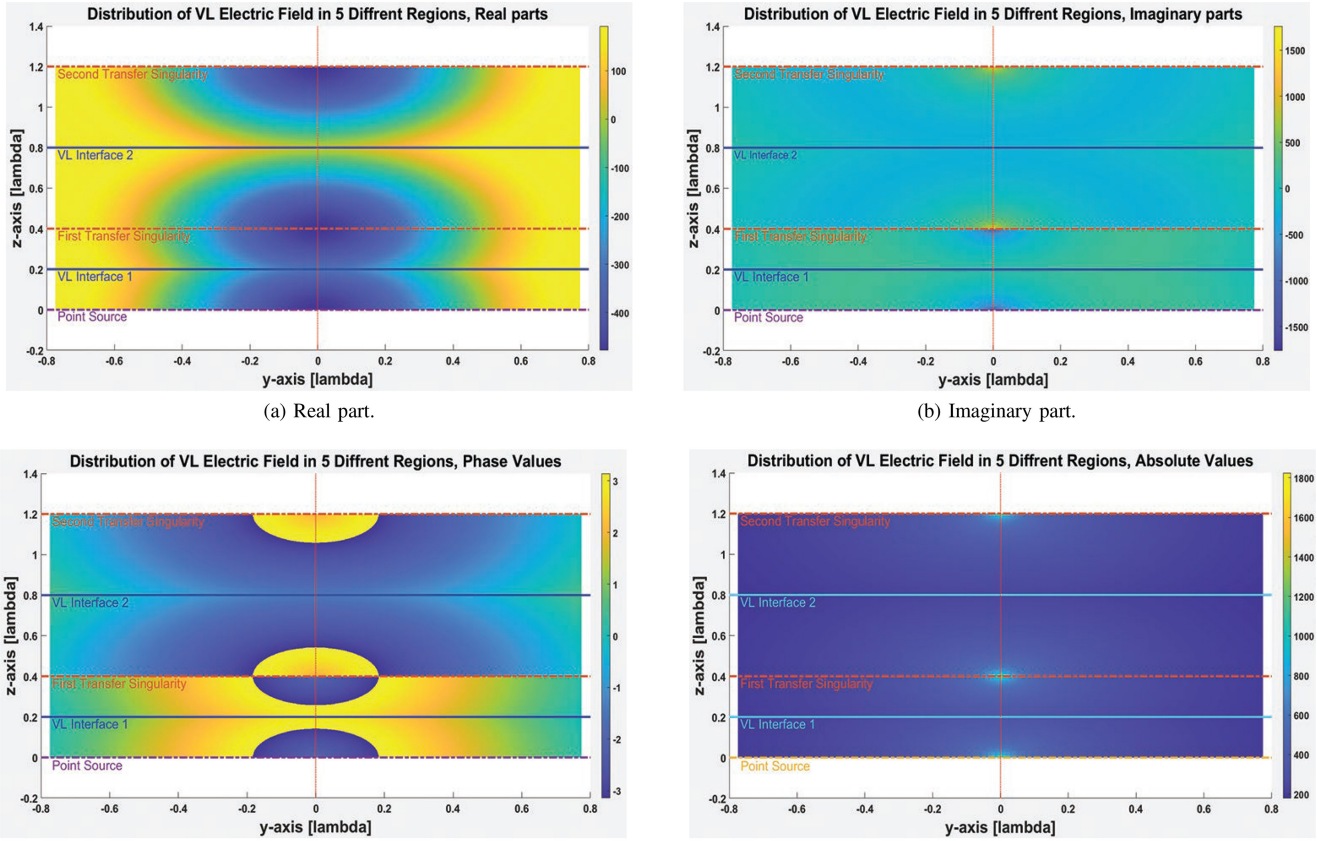

(a) Real part.

(b) Imaginary part.

(c) Phase.

(d) Magnitude.

FIGURE 6. Visualizations of the Electric field of a line-source in front of the VL.

the field as Kong's spectral-domain expressions in his 2002 paper [14]. On the other hand, for his 3D expressions, Kong does not split Regions II and III into two sub-regions relying instead on a single expression in each of these regions. Thus, Kong's expressions produce outgoing waves at both the singularity within the VL as well as at the external focus point. Our expressions provide a consistent flow of power across the transfer planes.

The Poynting vector for this ZED polarization can easily be found as

$$\bar{S}(\bar{r}|d_1,d) = \bar{E}(\bar{r}|d_1,d)\times\bar{H}^*(\bar{r}|d_1,d) = \eta\left[\frac{k_0 Il}{4\pi}\right]^2 \begin{cases} \frac{1}{r^2}\left\{\hat{r}\xi(r)\sin^2\theta + \hat{\theta}\zeta(r)\sin 2\theta\right\}, & z \le d_1 \\ -\frac{1}{r_1^2}\left\{\hat{r}_1\xi(r_1)\sin^2\theta_1 + \hat{\theta}_1\zeta(r_1)\sin 2\theta_1\right\}, & d_1 < z \le 2d_1 \\ \frac{1}{r_1^2}\left\{\hat{r}_1\xi^*(r_1)\sin^2\theta_1 + \hat{\theta}_1\zeta^*(r_1)\sin 2\theta_1\right\}, & 2d_1 \le z \le d_2 \\ -\frac{1}{r_2^2}\left\{\hat{r}_2\xi^*(r_2)\sin^2\theta_2 + \hat{\theta}_2\zeta^*(r_2)\sin 2\theta_2\right\}, & d_2 \le z < 2d \\ \frac{1}{r_2^2}\left\{\hat{r}_2\xi(r_2)\sin^2\theta_2 + \hat{\theta}_2\zeta(r_2)\sin 2\theta_2\right\}, & z > 2d, \end{cases} \tag{47}$$

where

$$\xi(r) = 1 + \left(\frac{j}{k_0 r}\right)^3 \text{ and } \zeta(r) = \frac{j}{k_0 r} - \left(\frac{j}{k_0 r}\right)^3 = \frac{j\xi^*(r)}{k_0 r}. \tag{48}$$

The time-average power density can be obtained as

$$\left\langle \bar{S}(\bar{r}|d_1,d)\right\rangle = \frac{1}{2}\Re\left\{\bar{S}(\bar{r},d_1,d)\right\} = \frac{\eta}{2}\left[\frac{k_0 Il}{4\pi}\right]^2 \begin{cases} \hat{r}\frac{1}{r^2}\sin^2\theta, & z \le d_1 \\ -\hat{r}_1\frac{1}{r_1^2}\sin^2\theta_1, & d_1 \le z < 2d_1 \\ \hat{r}_1\frac{1}{r_1^2}\sin^2\theta_1, & 2d_1 < z \le d_2 \\ -\hat{r}_2\frac{1}{r_2^2}\sin^2\theta_2, & d_2 \le z < 2d \\ \hat{r}_2\frac{1}{r_2^2}\sin^2\theta_2, & z > 2d. \end{cases} \tag{49}$$

As can be seen from the obtained relations in (49), the time-average Poynting power in region II-A is a vector with opposite direction to that of in region II-B. Therefore, as it is shown in Fig. (5), it can be concluded that the total time-average power emanating from any sphere centered at $\bar{r} = (0, 0, 2d_1)$ with a radius smaller than the minimum of d_1 and $d - d_1$ is zero. Alternatively, the total power entering from any hemisphere in Region II-A into the singularity is equal to the power emanating from the singularity out of any other hemisphere into Region II-B. This fact is true for the power in Regions III-A and III-B and any two hemispheres centered at $\bar{r} = (0, 0, 2d)$. This shows that the two singular points associated with our solution, inside and outside of the VL, are neither sources nor sinks, and justifies our denoting them as transfer singularities. This is a novel result that, to

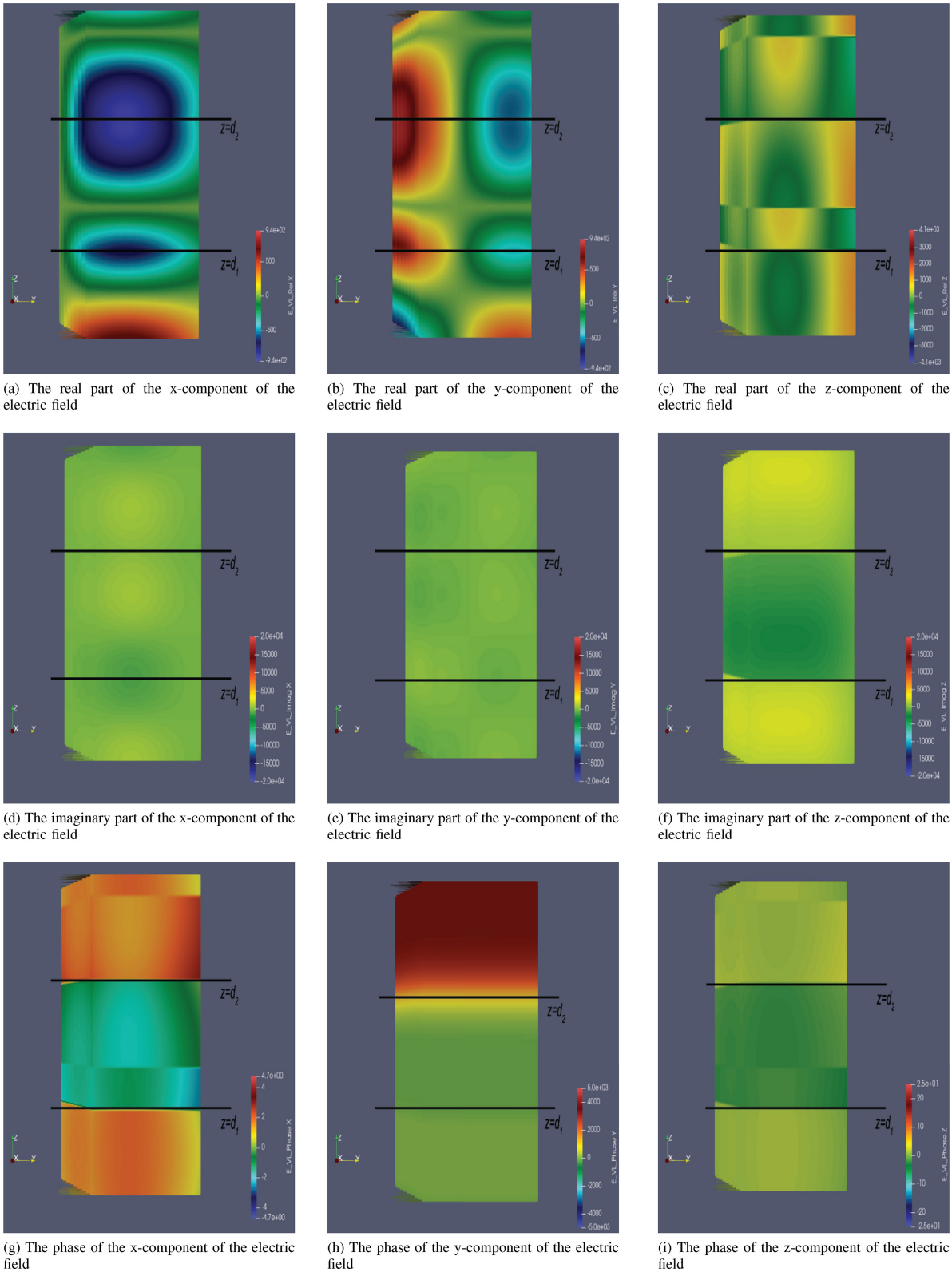

(a) The real part of the x-component of the electric field

(b) The real part of the y-component of the electric field

(c) The real part of the z-component of the electric field

(d) The imaginary part of the x-component of the electric field

(e) The imaginary part of the y-component of the electric field

(f) The imaginary part of the z-component of the electric field

(g) The phase of the x-component of the electric field

(h) The phase of the y-component of the electric field

(i) The phase of the z-component of the electric field

FIGURE 7. Visualization of the Electric field of a ZED in front of the VL.

the best of the authors' knowledge, has not been reported elsewhere in the literature.

Similar expressions can be obtained for the XED and YED. (See Appendix A.)

A. VISUALIZATION OF THE ELECTRIC FIELD

Fig. (6) depicts the real part, imaginary part, the phase and the absolute value of the electric field for an x-directed line-source using the 2D VL Green's function introduced in (31).

The line-source is located at the origin with the magnitude of the current chosen such that the coefficient becomes unity. The spatial units are depicted in terms of wavelength. The source is located in free-space in front of the VL having thickness $d = 0.3\lambda$ and $d_1 = 0.1\lambda$.

The singularity at the source is clearly visible in the imaginary part and the magnitude of the electric field. In addition, across the two transfer planes (lines in 2D) we see the flipping of the sign in the imaginary part and phase. The actual value of the field at these planes has not been plotted because of the uncertainty of the value of the field on these planes.

Fig. (7) illustrates the real part, imaginary part and the phase of the electric field distribution of a ZED polarization located at the origin of the Cartesian system of coordinates, with unity as the coefficient of the magnitude of the current. The thickness and distance from the lens is the same as in the 2D case. As can be seen from the plots the real and imaginary parts of the x and y-components of the field are continuous everywhere including the boundaries of the VL (these being the tangential components). For the 3D case, the z-component of the electric field is discontinuous across the lens boundaries and transfer planes. At the lens boundaries, because of the negative-sign flip in the relative permittivity, the z-component of the electric flux density remains continuous and does not require a supporting surface charge density. At the power-transfer planes there is no sign flip and therefore requires that we postulate a supporting surface charge density.

IV. CONCLUSION

We have derived 2D and 3D Green's functions corresponding to the electromagnetic field of a point-source in front of a slab of double-negative material constituting the ideal VL. These are given for a line-source in the 2D case and two polarizations of an electric dipole in the 3D case. The electromagnetic fields are given in terms of the scalar Green's function associated with a particular scalar BVP for each case. For convenience, the expressions are written in different systems of coordinates and can be easily utilized in inverse scattering work associated with microwave imaging. The occurrence of singularities in these expressions are rationalized as a new type of power-transfer singularity and do not present any logical grounds to deny the existence of such a lens. On the other hand, we find that all the fields suffer a complex-conjugate jump across the two power-transfer planes. For the case where the excitation produces a normal component of the electric field at these planes, we have found it necessary to postulate a problematic surface charge density. If such a charge density cannot be re-interpreted then this result goes against the realizability of an ideal VL.

APPENDIX A
SIMILAR RELATIONS FOR THE XED AND YED

XED polarization with current density $\bar{J}(\bar{r}) = \hat{x}Il\delta(\bar{r})$ located at the origin, again in front of a similarly defined VL. The electric field of the XED in the first region, where the point-source is located, following a procedure similar to that taken for the ZED polarization of (38) as

$$\bar{E}(\bar{r}|d_1, d) = \\ = -j\omega\mu_0\mu_r Il\left[\hat{x} + \frac{1}{k_0^2}\nabla\frac{\partial}{\partial x}\right]g(\bar{r}|\bar{r}_0, d_1, d)\hat{x}. \quad (50)$$

Introducing the 3D Green's function $g(\bar{r}|\bar{r}_0, d_1, d)$ introduced in (33) for an XED, and taking the required partial derivatives in (50), taking care to consider the change of sign of the permeability inside the VL, gives rise to the following expression for the electric field as

$$\bar{E}(\bar{r}|d_1, d) = \frac{-j\omega\mu_0 Il}{4\pi} \begin{cases} \left\{\hat{x}\frac{1}{r}\alpha(r) - \frac{x}{r^3}\beta(r)\bar{r}\right\}e^{-jk_0 r}, & z \le d_1 \\ \left\{\hat{x}\frac{1}{r_1}\alpha(r_1) - \frac{x}{r_1^3}\beta(r_1)\bar{r}_1\right\}e^{-jk_0 r_1}, & d_1 \le z < 2d_1 \\ \left\{\hat{x}\frac{1}{r_1}\alpha^*(r_1) - \frac{x}{r_1^3}\beta^*(r_1)\bar{r}_1\right\}e^{jk_0 r_1}, & 2d_1 < z \le d_2 \\ \left\{\hat{x}\frac{1}{r_2}\alpha^*(r_2) - \frac{x}{r_2^3}\beta^*(r_2)\bar{r}_2\right\}e^{jk_0 r_2}, & d_2 \le z < 2d \\ \left\{\hat{x}\frac{1}{r_2}\alpha(r_2) - \frac{x}{r_2^3}\beta(r_2)\bar{r}_2\right\}e^{-jk_0 r_2}, & z > 2d, \end{cases} \quad (51)$$

where $\alpha(r)$ and $\beta(r)$ are defined as in (40). Equivalently, noting that $\hat{x} = \hat{\rho}\cos\phi - \hat{\phi}\sin\phi$, (51) can be written in cylindrical coordinates as

$$\bar{E}(\bar{r}|d_1, d) = \frac{-j\omega\mu_0 Il}{4\pi} \begin{cases} \left\{-\hat{\phi}\sin\phi\alpha(r) + \hat{\rho}\cos\phi\left[\alpha(r) - \frac{\rho^2}{r^2}\beta(r)\right] \right. \\ \quad \left. -\hat{z}\frac{\rho z}{r^2}\beta(r)\right\}\frac{e^{-jk_0 r}}{r}, & z \le d_1 \\ \left\{-\hat{\phi}\sin\phi\alpha(r_1) + \hat{\rho}\cos\phi\left[\alpha(r_1) - \frac{\rho^2}{r_1^2}\beta(r_1)\right] \right. \\ \quad \left. -\hat{z}\frac{\rho(z-2d_1)}{r_1^2}\beta(r_1)\right\}\frac{e^{-jk_0 r_1}}{r_1}, & d_1 \le z < 2d_1 \\ \left\{-\hat{\phi}\sin\phi\alpha^*(r_1) + \hat{\rho}\cos\phi\left[\alpha^*(r_1) - \right.\right. \\ \quad \left.\left. \frac{\rho^2}{r_1^2}\beta^*(r_1)\right] - \hat{z}\frac{\rho(z-2d_1)}{r_1^2}\beta^*(r_1)\right\}\frac{e^{jk_0 r_1}}{r_1}, & 2d_1 < z \le d_2 \\ \left\{-\hat{\phi}\sin\phi\alpha^*(r_1) + \hat{\rho}\cos\phi\left[\alpha^*(r_1) - \right.\right. \\ \quad \left.\left. \frac{\rho^2}{r_1^2}\beta^*(r_1)\right] - \hat{z}\frac{\rho(z-2d_1)}{r_1^2}\beta^*(r_1)\right\}\frac{e^{jk_0 r_1}}{r_1}, & d_2 \le z < 2d \\ \left\{-\hat{\phi}\sin\phi\alpha(r_2) + \hat{\rho}\cos\phi[\alpha(r_2) - \right. \\ \quad \left. \frac{\rho^2}{r_2^2}\beta(r_2)\right] - \hat{z}\frac{\rho z}{r_2^2}\beta(r_2)\right\}\frac{e^{-jk_0 r_2}}{r_2}, & z > 2d. \end{cases} \quad (52)$$

Using $\hat{x} = \hat{r}\sin\theta\cos\phi + \hat{\theta}\cos\theta\cos\phi - \hat{\phi}\sin\phi$, which is valid in the θ, θ_1, and θ_2 variables as well, this can easily be written in spherical coordinates as

$$\bar{E}(\bar{r}|d_1, d) = \frac{-j\omega\mu_0 Il}{4\pi}$$

$$\begin{cases} \Big\{\hat{r}[\alpha-\beta](r)\sin\theta\cos\phi+\hat{\theta}\,\alpha(r) \\ \quad \cos\theta\cos\phi-\hat{\phi}\,\alpha(r)\sin\phi\Big\}\frac{e^{-jk_0r}}{r}, & z\le d_1 \\ \Big\{\hat{r}_1[\alpha-\beta](r_1)\sin\theta_1\cos\phi+\hat{\theta}_1\,\alpha(r_1) \\ \quad \cos\theta_1\cos\phi-\hat{\phi}\,\alpha(r_1)\sin\phi\Big\}\frac{e^{-jk_0r_1}}{r_1}, & d_1\le z<2d_1 \\ \Big\{\hat{r}_1[\alpha-\beta]^*(r_1)\sin\theta_1\cos\phi+\hat{\theta}_1\,\alpha^*(r_1) \\ \quad \cos\theta_1\cos\phi-\hat{\phi}\,\alpha^*(r_1)\sin\phi\Big\}\frac{e^{jk_0r_1}}{r_1}, & 2d_1<z\le d_2 \\ \Big\{\hat{r}_2[\alpha-\beta]^*(r_2)\sin\theta_2\cos\phi+\hat{\theta}_2\,\alpha^*(r_2) \\ \quad \cos\theta_2\cos\phi-\hat{\phi}\,\alpha^*(r_2)\sin\phi\Big\}\frac{e^{jk_0r_2}}{r_2}, & d_2\le z<2d \\ \Big\{\hat{r}_2[\alpha-\beta](r_2)\sin\theta_2\cos\phi+\hat{\theta}_2\,\alpha(r_2) \\ \quad \cos\theta_2\cos\phi-\hat{\phi}\,\alpha(r_2)\sin\phi\Big\}\frac{e^{-jk_0r_2}}{r_2}, & z>2d, \end{cases} \tag{53}$$

where $[\alpha-\beta]$ and $[\alpha-\beta]^*$ are as defined in (43).

Applying Faraday's law to the electric field obtained in (51) leads to the magnetic field:

$$\bar{H}(\bar{r}|d_1,d)=\frac{1}{-j\omega\mu_0\mu_r}\nabla\times\bar{E}(\bar{r},d_1,d)=\frac{Il}{4\pi}$$
$$\begin{cases} \Big\{\frac{1}{r^2}\gamma(r)\big[\hat{y}z-\hat{z}y\big]\Big\}e^{-jk_0r}, & z\le d_1 \\ -\Big\{\frac{1}{r_1^2}\gamma(r_1)\big[\hat{y}(z-2d_1)-\hat{z}y\big]\Big\}e^{-jk_0r_1}, & d_1\le z<2d_1 \\ -\Big\{\frac{1}{r_1^2}\gamma^*(r_1)\big[\hat{y}(z-2d_1)-\hat{z}y\big]\Big\}e^{jk_0r_1}, & 2d_1<z\le d_2 \\ \Big\{\frac{1}{r_2^2}\gamma^*(r_2)\big[\hat{y}(z-2d)-\hat{z}y\big]\Big\}e^{jk_0r_2}, & d_2\le z<2d \\ \Big\{\frac{1}{r_2^2}\gamma(r_2)\big[\hat{y}(z-2d)-\hat{z}y\big]\Big\}e^{-jk_0r_2}, & z>2d, \end{cases} \tag{54}$$

where γ and γ^* are as defined in (45). Equivalently, this can be written in spherical coordinates as

$$\bar{H}(\bar{r}|d_1,d)=\frac{Il}{4\pi}$$
$$\begin{cases} \gamma(r)\Big[\hat{\theta}\sin\phi+\hat{\phi}\cos\theta\cos\phi\Big]\frac{e^{-jk_0r}}{r}, & z\le d_1 \\ -\gamma(r_1)\Big[\hat{\theta}_1\sin\phi+\hat{\phi}\cos\theta_1\cos\phi\Big]\frac{e^{-jk_0r_1}}{r_1}, & d_1\le z<2d_1 \\ -\gamma^*(r_1)\Big[\hat{\theta}_1\sin\phi+\hat{\phi}\cos\theta_1\cos\phi\Big]\frac{e^{jk_0r_1}}{r_1}, & 2d_1\le z\le d_2 \\ \gamma^*(r_2)\Big[\hat{\theta}_2\sin\phi+\hat{\phi}\cos\theta_2\cos\phi\Big]\frac{e^{jk_0r_2}}{r_2}, & d_2\le z<2d \\ \gamma(r_2)\Big[\hat{\theta}_2\sin\phi+\hat{\phi}\cos\theta_2\cos\phi\Big]\frac{e^{-jk_0r_2}}{r_2}, & z>2d, \end{cases} \tag{55}$$

where now, again, $\hat{y}=\hat{r}\sin\theta\sin\phi+\hat{\theta}\cos\theta\sin\phi+\hat{\phi}\cos\phi$, and also $\hat{z}=\hat{r}\cos\phi-\hat{\theta}\sin\theta$ are valid in the shifted systems. Notice that for the XED polarization, and similarly for the YED polarization, at the two power transfer planes there is no normal component of the electric field. Thus, although all the fields suffer a complex-conjugate jump across these planes, there is no surface charge generated that needs to be explained.

The Poynting vector for the XED can be found as

$$\bar{S}(\bar{r}|d_1,d)=\eta\Big[\frac{k_0Il}{4\pi}\Big]^2$$
$$\begin{cases} \frac{1}{r^2}\Big\{\hat{r}\,\xi(r)[\cos^2\theta\cos^2\phi+\sin^2\phi]-\hat{\theta} \\ \zeta(r)\sin2\theta\cos^2\phi+\hat{\phi}\,\zeta(r)\sin\theta\cos2\phi\Big\}, & z\le d_1 \\ -\frac{1}{r_1^2}\Big\{\hat{r}_1\,\xi(r_1)[\cos^2\theta_1\cos^2\phi+\sin^2\phi]-\hat{\theta}_1 \\ \zeta(r_1)\sin2\theta_1\cos^2\phi+\hat{\phi}\,\zeta(r_1)\sin\theta_1\cos2\phi\Big\}, & d_1\le z<2d_1 \\ \frac{1}{r_1^2}\Big\{\hat{r}_1\,\xi^*(r_1)[\cos^2\theta_1\cos^2\phi+\sin^2\phi]-\hat{\theta}_1 \\ \zeta^*(r_1)\sin2\theta_1\cos^2\phi+\hat{\phi}\,\zeta^*(r_1)\sin\theta_1\cos2\phi\Big\}, & 2d_1<z\le d_2 \\ -\frac{1}{r_2^2}\Big\{\hat{r}_2\,\xi^*(r_2)[\cos^2\theta_2\cos^2\phi+\sin^2\phi]-\hat{\theta}_2 \\ \zeta^*(r_2)\sin2\theta_2\cos^2\phi+\hat{\phi}\,\zeta^*(r_2)\sin\theta_2\cos2\phi\Big\}, & d_2\le z<2d \\ \frac{1}{r_2^2}\Big\{\hat{r}_2\,\xi(r_2)[\cos^2\theta_2\cos^2\phi+\sin^2\phi]-\hat{\theta}_2 \\ \zeta(r_2)\sin2\theta_2\cos^2\phi+\hat{\phi}\,\zeta(r_2)\sin\theta_2\cos2\phi\Big\}, & z>2d, \end{cases} \tag{56}$$

where ξ and ζ are as defined in (48). Finally the time-average power density can be obtained from (56) as

$$\big\langle\bar{S}(\bar{r}|d_1,d)\big\rangle=\frac{1}{2}\Re\big\{\bar{S}(\bar{r}|d_1,d)\big\}$$
$$=\frac{\eta}{2}\Big[\frac{k_0Il}{4\pi}\Big]^2\begin{cases} \hat{r}\frac{1}{r^2}[\cos^2\theta\cos^2\phi+\sin^2\phi], & z\le d_1 \\ -\hat{r}_1\frac{1}{r_1^2}[\cos^2\theta_1\cos^2\phi+\sin^2\phi], & d_1\le z<2d_1 \\ \hat{r}_1\frac{1}{r_1^2}[\cos^2\theta_1\cos^2\phi+\sin^2\phi], & 2d_1<z\le d_2 \\ -\hat{r}_2\frac{1}{r_2^2}[\cos^2\theta_2\cos^2\phi+\sin^2\phi], & d_2\le z<2d \\ \hat{r}_2\frac{1}{r_2^2}[\cos^2\theta_2\cos^2\phi+\sin^2\phi], & z>2d, \end{cases} \tag{57}$$

Finally, the YED polarization with current density $\bar{J}(\bar{r})=\hat{y}Il\delta(\bar{r})$, can be obtained from the XED relations by changing ϕ to $-\frac{\pi}{2}+\phi$, so we do not repeat them here.

REFERENCES

[1] V. G. Veselago, "The electrodynamics of substances with simultaneously negative values of ε and μ," *Phys. Uspekhi*, vol. 10, no. 4, pp. 509–514, 1968.

[2] J. B. Pendry, "Negative refraction makes a perfect lens," *Phys. Rev. Lett.*, vol. 85, no. 18, p. 3966, 2000.

[3] D. R. Smith, W. J. Padilla, D. Vier, S. C. Nemat-Nasser, and S. Schultz, "Composite medium with simultaneously negative permeability and permittivity," *Phys. Rev. Lett.*, vol. 84, no. 18, p. 4184, 2000.

[4] R. A. Shelby, D. R. Smith, and S. Schultz, "Experimental verification of a negative index of refraction," *Science*, vol. 292, no. 5514, pp. 77–79, 2001.

[5] J. B. Pendry and D. R. Smith, "Reversing light with negative refraction," *Phys. Today*, vol. 57, no. 6, pp. 37–43, 2004.

[6] G. V. Eleftheriades and K. G. Balmain, *Negative-Refraction Metamaterials: Fundamental Principles and Applications*. Hoboken, NJ, USA: Wiley, 2005.

[7] N. Engheta and R. W. Ziolkowski, *Metamaterials: Physics and Engineering Explorations*. Hoboken, NJ, USA: Wiley, 2006.

[8] N. Garcia and M. Nieto-Vesperinas, "Left-handed materials do not make a perfect lens," *Phys. Rev. Lett.*, vol. 88, no. 20, 2002, Art. no. 207403.

[9] D. Maystre and S. Enoch, "Perfect lenses made with left-handed materials: Alice's mirror?" *J. Opt. Soc. Amer. A Opt. Image Sci. Vis.*, vol. 21, no. 1, pp. 122–131, 2004.

[10] S. A. Ramakrishna, J. Pendry, D. Schurig, D. Smith, and S. Schultz, "The asymmetric lossy near-perfect lens," *J. Mod. Opt.*, vol. 49, no. 10, pp. 1747–1762, 2002.

[11] A. N. Lagarkov and V. N. Kissel, "Near-perfect imaging in a focusing system based on a left-handed-material plate," *Phys. Rev. Lett.*, vol. 92, no. 7, 2004, Art. no. 077401.

[12] J. Valentine *et al.*, "Three-dimensional optical metamaterial with a negative refractive index," *Nature*, vol. 455, no. 7211, pp. 376–379, 2008.

[13] R. E. Collin, "Frequency dispersion limits resolution in veselago lens," *Progr. Electromagn. Res.*, vol. 19, pp. 233–261, May 2010.

[14] J. A. Kong, "Electromagnetic wave interaction with stratified negative isotropic media," *Progr. Electromagn. Res.*, vol. 35, pp. 1–52, 2002.
[15] F. Mesa, M. Freire, R. Marqués, and J. Baena, "Three-dimensional superresolution in metamaterial SLAB lenses: Experiment and theory," *Phys. Rev. B, Condens. Matter*, vol. 72, no. 23, 2005, Art. no. 235117.
[16] X. Zhang and Z. Liu, "Superlenses to overcome the diffraction limit," *Nat. Mater.*, vol. 7, no. 6, pp. 435–441, 2008.
[17] D. Lu and Z. Liu, "Hyperlenses and metalenses for far-field superresolution imaging," *Nat. Commun.*, vol. 3, no. 1, pp. 1–9, 2012.
[18] A. K. Iyer and G. V. Eleftheriades, "Free-space imaging beyond the diffraction limit using a veselago-pendry transmission-line metamaterial superlens," *IEEE Trans. Antennas Propag.*, vol. 57, no. 6, pp. 1720–1727, Jun. 2009.
[19] J. Aronsson and V. Okhmatovski, "Comparison of numerical approaches to the evaluation of Veselago lens' green's function," in *Proc. IEEE Int. Symp. Antennas Propag. (APSURSI)*, 2011, pp. 1519–1521.
[20] V. Okhmatovski, J. Aronsson, and L. Shafai, "A well-conditioned noniterative approach to solution of the inverse problem," *IEEE Trans. Antennas Propag.*, vol. 60, no. 5, pp. 2418–2430, May 2012.
[21] K. P. Gaikovich, "Left-handed lens tomography and holography," *Inverse Probl. Sci. Eng.*, vol. 28, no. 3, pp. 296–313, 2020.
[22] D. Schrig, "Metamaterial electromagnetic cloak at microwave frequencies," *Science*, vol. 314, no. 5801, pp. 977–980, 2006.
[23] T. Chen, S. Li, and H. Sun, "Metamaterials application in sensing," *Sensors*, vol. 12, no. 3, pp. 2742–2765, 2012.
[24] S. Raghavan and V. Rajeshkumar, "An overview of metamaterials in biomedical applications," *Progr. Electromagn. Res*, vol. 25, p. 369, Mar. 2013.
[25] S. I. Rosaline and S. Raghavan, "Survey on metamaterials in biomedicine," in *Proc. IEEE Int. Conf. Comput. Intell. Comput. Res.*, 2013, pp. 1–4.
[26] A. Sihvola, "Enabling optical analog computing with metamaterials," *Science*, vol. 343, no. 6167, pp. 144–145, 2014.
[27] Z. Chen, B. Guo, Y. Yang, and C. Cheng, "Metamaterials-based enhanced energy harvesting: A review," *Physica B Condens. Matter*, vol. 438, pp. 1–8, Apr. 2014.
[28] S. R. Sklan and B. Li, "Thermal metamaterials: Functions and prospects," *Nat. Sci. Rev.*, vol. 5, no. 2, pp. 138–141, 2018.
[29] A. Menshov and V. I. Okhmatovski, "Superlens enhanced 2-D microwave tomography with contrast source inversion method," *IEEE Open J. Antennas Propag.*, vol. 2, pp. 453–463, 2021.
[30] R. F. Harrington, "Time-harmonic," in *Electromagnetic Fields*. Hoboken, NJ, USA: Wiley, 2001, pp. 168–171.
[31] J. Minkel, "Left-handed materials debate heats up," *Physics*, vol. 9, p. 23, May 2002.
[32] G. W. Milton, N.-A. P. Nicorovici, R. C. McPhedran, and V. A. Podolskiy, "A proof of superlensing in the quasistatic regime, and limitations of superlenses in this regime due to anomalous localized resonance," *Proc. Roy. Soc. A Math. Phys. Eng. Sci.*, vol. 461, no. 2064, pp. 3999–4034, 2005.
[33] U. Leonhardt and T. Philbin, "General relativity in electrical engineering," in *Proc. Metamaterials II*, vol. 6581, 2007, Art. no. 658104.
[34] P. Valanju, R. Walser, and A. Valanju, "Wave refraction in negative-index media: Always positive and very inhomogeneous," *Phys. Rev. Lett.*, vol. 88, no. 18, 2002, Art. no. 187401.
[35] D. Smith, D. Schurig, and J. Pendry, "Negative refraction of modulated electromagnetic waves," *Appl. Phys. Lett.*, vol. 81, no. 15, pp. 2713–2715, 2002.

MARZIEH EINI KELESHTERI (Graduate Student Member, IEEE) received the M.Sc. degree in pure mathematics from the University of Isfahan, Iran, in 2007, and the M.Sc. degree in applied mathematics and computer sciences and the first Ph.D. degree in mathematics from Eastern Mediterranean University, North Cyprus, in 2011 and 2015, respectively. She is currently pursuing the second Ph.D. degree in electrical engineering with the University of Manitoba, Canada. Her current research interests are inverse problems, boundary value problems, and partial differential equations arising in microwave imaging. She has served as the Vice-Chair of IEEE Women in Engineering, Winnipeg section since September 2019. She has received several prestigious awards, including the Price Graduate Scholarships for Women in Engineering in 2019.

VLADIMIR I. OKHMATOVSKI (Senior Member, IEEE) was born in Moscow, Russia, in 1974. He received the M.S. degree (with Distinction) in radiophysics and Ph.D. degree in antennas and microwave circuits from the Moscow Power Engineering Institute, Moscow, Russia, in 1996 and 1997, respectively.

In 1997, he joined the Radio Engineering Department, Moscow Power Engineering Institute, as an Assistant Professor. He was a Postdoctoral Research Associate with the National Technical University of Athens from 1998 to 1999 and with the University of Illinois at Urbana-Champaign from 1999 to 2003. From 2003 to 2004, he was with the Department of Custom Integrated Circuits, Cadence Design Systems, as a Senior Member of Technical Staff, and from 2004 to 2008 as an Independent Consultant. In 2004, he joined the Department of Electrical and Computer Engineering, University of Manitoba, Winnipeg, MB, Canada, where is currently a Full Professor. He is a Registered Professional Engineer in the Province of Manitoba, Canada. His research interests are the fast algorithms of electromagnetics, high-performance computing, modeling of interconnects, and inverse problems. He authored and coauthored over 150 technical papers, book chapters, and patents in the areas of computational and applied electromagnetics.

Prof. Okhmatovski was a recipient of the 2017 Intel Corporate Research Council Outstanding Researcher Award, the 1995 Scholarship of the Government of Russian Federation, and the 1996 scholarship of the President of the Russian Federation. He was the recipient of the 1996 Best Young Scientist Report of the VI International Conference on Mathematical Methods in Electromagnetic Theory. He was also a co-recipient of the Best Paper Award at the 3rd Electronic Packaging Technology Conference in 2001 and the Outstanding ACES Journal Paper Award in 2007. Since 2017, has been served on the Technical Program Review Committee of the IEEE Microwave Theory and Techniques Society (IEEE MTT-S) International Microwave Symposium, and since 2020 on IEEE MTT-S Technical Committee on Field Theory and Computational Electromagnetics. He was a TPC Co-Chair of 2021 Applied and Computational Electromagnetics Society Symposium. He has been an Active Volunteer for the IEEE Antennas and Propagation Society (IEEE AP-S) as well as IEEE MTT-S serving as a Chapter Chair of the IEEE Winnipeg Waves Chapter from 2006 to 2011 and has been a Chair and a Co-Chair of the Membership and Benefits Committee of the IEEE AP-S since 2018. In 2022, he serves as the Co-Chair of the Packaging Benchmarks Committee within the IEEE Electronics Packaging Society.

JOE LOVETRI (Senior Member, IEEE) received the Ph.D. degree from the University of Ottawa in 1991. From 1984 to 1986, he was an EMI/EMC Engineer with Sperry Defence Division in Winnipeg and from 1986 to 1988 he held the position of TEMPEST Engineer with Communications Security Establishment in Ottawa. From 1988 to 1991, he was a Research Officer with the Institute for Information Technology, National Research Council of Canada. His academic career began in 1991, when he joined the Department of Electrical and Computer Engineering, University of Western Ontario, where he remained until 1999. From 1997 to 1998, he spent a sabbatical year with the TNO Physics and Electronics Laboratory, The Netherlands, doing research in time-domain computational methods and ground-penetrating RADAR. In 1999, he joined the University of Manitoba where he is currently a Professor with the Department of Electrical and Computer Engineering. From 2004 to 2009, he was the Associate Dean of the Research and Graduate Programs with the Faculty of Engineering. From 2013 to 2020, he was the Head of the ECE Department. He has been a Registered Professional Engineer since 1994. His main research interests lie in the areas of microwave and ultrasound imaging, computational electromagnetics, and inverse problems. He received the URSI Young Scientist Award, in 1993, the 2000 IEEE EMC Best Symposium Paper Award, and the 2007 ACES Outstanding Paper Award, the University of Manitoba Rh Award for Outstanding Contributions to Scholarship and Research in the Applied Sciences in 2002. From 2005 to 2009, he was the National Representative for Commission E on the Canadian National Committee of URSI. He has been a Chapter Chair for the IEEE EMC Ottawa Chapter as well as the Winnipeg Waves Chapter (AP/MTT).